Journal of Alloys and Compounds 489 (2010) 130–135

Contents lists available at ScienceDirect

Journal of Alloys and Compounds

journal homepage: www.elsevier.com/locate/jallcom

Phase stability, mechanical property, and electronic structure of Mg–Li system

Chao Ping Liang, Hao Ran Gong*

State Key Laboratory of Powder Metallurgy, Central South University, Changsha, Hunan 410083, China

ARTICLE INFO

Article history:
Received 30 June 2009
Received in revised form 6 September 2009
Accepted 7 September 2009
Available online 15 September 2009

Keywords:
Metals and alloys
Crystal structure
Elasticity
Phase transitions
Computer simulations

ABSTRACT

First principle calculation reveals that the HCP, BCC, and FCC $Mg_{100-x}Li_x$ phases are energetically favorable with negative heats of formation, and are predicted to be the most stable structures at 0 K when $0 \leq x < 18$, $18 \leq x < 73$, and $73 \leq x \leq 100$, respectively. Calculation also shows that for Mg–Li phases there is an almost linear variation of bulk moduli with composition, and crystal structure has only a little effect on bulk moduli. In addition, it is found that Mg_3Li and MgLi have phase sequences of BCC → HCP → FCC and BCC → FCC under high pressure, respectively, and that the anomalous mechanical instability of the HCP MgLi phase would be attributed to its weak bonding and step-like electronic structure of valence bands.

1. Introduction

During the past decades, the binary alloy system of Mg–Li has raised great research interests due to its unique structural, mechanical, electrical and thermal properties, etc. It is well known that the simple metals of Li and Mg are regarded as alkali and alkaline-earth metals with only one and two conduction s-electrons, respectively. The phase transitions of the Mg–Li system at low temperature, however, have been found to be complicated and attractive for many years among scientists. For instance, in 1947, Barrett [1] first discovered that the body-centered-cubic (BCC) Li was transformed to the structure of face-centered-cubic (FCC) under cold working at low temperature. Later, Barrett and Trautz [2,3] found that both Li and Mg–Li alloys underwent a martensitic transformation on cooling below 70 K and suggested that the new phase was hexagonal-close-packed (HCP). In 1990s, both Crisp and Maier et al. observed that the Mg–Li alloys were transformed to a close-packed rhombohedral structure (9R) at liquid helium temperature and such a structure was identified to be a low-temperature martensitic phase [4,5].

Another interesting aspect of the Mg–Li system is that it could be regarded as a kind of ultralight materials with high specific strength, and is a promising candidate for commercial transport, aerospace and high-performance applications [6–10]. For example, the Mg–Li alloys were reinforced as a composite matrix by a series of fibers such as carbon, alumina and silicon carbide [7,8]. Recently, Furui et al. found that the Mg–Li alloys exhibited excellent superplastic properties during processing [10]. Moreover, the mechanical properties of various Mg–Li alloys were measured experimentally [11,12]. It was found that the elastic constants of Mg–Li alloys decreased with the increase of the Li content [11], and there was a nonlinear variation of elastic constants with temperature [12]. In addition, the Mg–Li alloys were also discovered to possess interesting electrical, thermal, and surface properties, etc. [13–15].

To understand the intrinsic mechanism of various properties of Mg–Li phases, it is of importance to investigate the Mg–Li system at an electronic scale theoretically. Regarding this respect, however, there are only several theoretical calculations of the Mg–Li system in the literature [16–19]. For instance, the structural and thermochemical properties of MgLi alloys were studied by means of pseudopotential methods [16], and the electronic structures of B2 and B32 MgLi were calculated through a linear combination of atomic orbitals method [17]. Very recently, Counts et al. obtained the mechanical properties of various BCC Mg–Li alloys by means of first principles calculations [18]. It should be pointed out that there is a lack of a thorough and systematic study of the correlation between various properties and structures of MgLi phases in the literature. The present study is therefore dedicated to investigate the structural stability, mechanical properties, high-pressure phase transition, and electronic structures of the Mg–Li system through first principles calculation.

2. Calculation methods

The first principles calculation is based on the well-established Vienna *ab initio* simulation package (VASP) within the density functional theory [20]. The calculation is conducted in a plane-

* Corresponding author. Tel.: +86 731 88877387; fax: +86 731 88710855.
E-mail address: gonghr@gmail.com (H.R. Gong).

0925-8388/$ – see front matter © 2009 Elsevier B.V. All rights reserved.
doi:10.1016/j.jallcom.2009.09.032

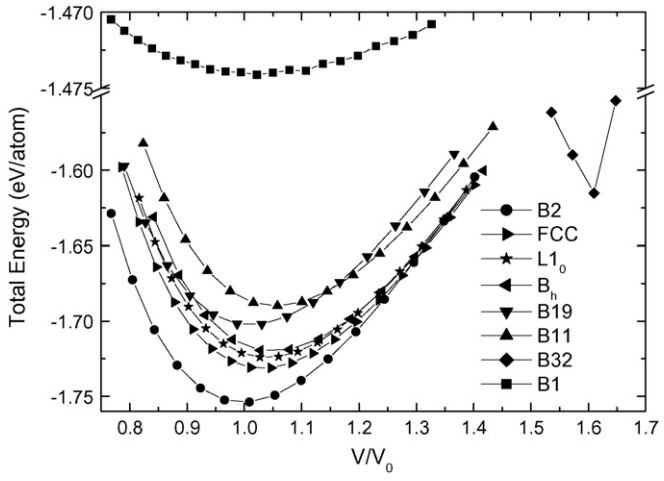

Fig. 1. Calculated total energies of the MgLi phases with crystal structures of B2, FCC, $L1_0$, B_h, B19, B11, B32 and B1, respectively, as a function of the ratio of volume (V/V_0, V_0 is the equilibrium volume of the B2 phase).

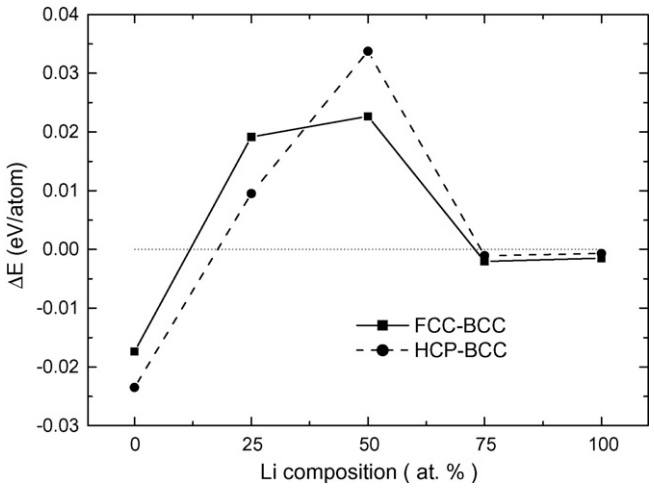

Fig. 2. Total energy differences (ΔE) of HCP (circle symbol) and FCC (square symbol) MgLi phases with respect to BCC as a function of Li composition, respectively. The dotted line is the line of zero.

wave basis, using the projector-augmented wave (PAW) method [21]. The exchange and correlation items are described by generalized gradient approximation (GGA) of Perdew et al. [22] and the cutoff energies are 300 and 450 eV for plane-wave basis and augmentation charge, respectively. In each calculation, periodic boundary conditions are added in three directions of the unit cell, and the energy criteria during the relaxation calculation are 0.01 and 0.1 meV for electronic and ionic relaxations, respectively, while the energy criterion is 0.001 meV for the calculation of density of states (DOS) and elastic constants.

At the very beginning, we did a series of test calculations, such as the k-point convergence test. As a result, the k-mesh of $13 \times 13 \times 13$ was adopted for all calculations. For k space integration, the temperature smearing method of Methfessel–Paxton [23] was used for dynamical calculation and the modified tetrahedron method of Blöchl–Jepsen–Andersen [24] was performed for static calculation.

3. Results and discussion

3.1. Structural stability

In order to find out the ground-state crystal structure of the Mg–Li system, five compositions, i.e., Mg_3Li, MgLi, $MgLi_3$, pure Mg and Li, with several possible ordered structures are selected for total energy calculations. As a typical example, Fig. 1 shows the correlation between the total energy and the ratio of volume (V/V_0) for these MgLi phases. One sees from the figure that the MgLi phase with a B2 (BCC lattice) structure has the lowest total energy and is therefore predicted to be the most stable structure corresponding to the ground state. Similarly, the A3 (HCP lattice), A1 (FCC lattice), $D0_3$ (BCC lattice), and $L1_2$ (FCC lattice) are predicted to be the ground-state structures of Mg, Li, Mg_3Li, and $MgLi_3$ phases, respectively (figures not shown). For convenience, the Bravais lattice symbols (FCC, BCC and HCP), instead of the *Strukturbericht* types, are adopted in the following text, tables, and figures. Accordingly, Table 1 lists the calculated physical properties of these Mg–Li phases with three common structures (BCC, FCC and HCP) as well as relevant experimental data [25]. From this table, it is evident that the most stable structures of these five Mg–Li phases predicted from the present calculations match well with experimental observations, and their lattice constants are also consistent with experimental data within an error of 1–2%. Moreover, the structural energy differences (ΔE) of these Mg–Li phases are derived and listed in Table 1. It is of interest to see that the ΔE in the Mg-rich region is bigger than those in the Li-rich region.

To further reveal the structural stability of the Mg–Li system, the above five Mg–Li phases are expressed as the form of $Mg_{100-x}Li_x$ (x is the atomic composition of Li), and the total energy differences of the FCC and HCP $Mg_{100-x}Li_x$ phases with respect to the BCC structures are calculated and are shown in Fig. 2. It can be observed from this figure that the HCP structure has lower total energy than the BCC and FCC structures when $0 \le x < 18$, the BCC structure is more stable than the other two structures when $18 \le x < 73$, while the FCC structure is energetically more favorable when $73 \le x \le 100$. It is of interest to compare the above results with similar experimental and theoretical observations in the literature [3,16,25–28]. By means of thermodynamic methods, Nayeb-Hashemi et al. [25] discovered that the HCP structure began to transform to the BCC structure at room temperature when $x > 17$, and such a transition was finished when $x > 30$. Moreover, Barrett [3] observed that the BCC structure is stable at low temperature when $x < 74$. Using the pseudopotential method, Hafner [16] found that the HCP $Mg_{100-x}Li_x$ structure has the lowest energy when $0 \le x < 20$ and $80 \le x \le 100$, while the BCC and FCC structures are energetically more favorable when $20 \le x < 65$ and $65 \le x < 80$, respectively. Through a careful comparison, it can be observed that that the calculated structural stability of the Mg–Li system from the present study matches well with the above experimental observations [3,25], and is in general agreement with the theoretical predictions [16]. It should be pointed out that there is a discrepancy regarding the structural stability of the Li-rich $Mg_{100-x}Li_x$ phases, i.e., HCP was predicted to be the most stable structure when $80 \le x \le 100$ by Hafner [16], while FCC is predicted when $73 \le x \le 100$ from the present study. Such a discrepancy would be probably due to the different theoretical methods used in the calculations, i.e., the pseudopotential method by Hafner [16] and the PAW method in the present study. Interestingly, the most stable FCC structure of pure Li derived from the present study is in good agreement with experimental observations of the low-temperature FCC structure by Barrett [1] and Dugdale et al. [26], and is consistent with similar theoretical results by Staikov et al. with a pseudopotential approach [27] and by Boettger and Trickey through a linear combination of Gaussian type orbital [28].

The heat of formation, ΔH_f, is derived according to the following formula:

$$\Delta H_f = \frac{E_{Mg_mLi_n} - mE_{Mg} - nE_{Li}}{m+n} \quad (1)$$

where $E_{Mg_mLi_n}$, E_{Mg} and E_{Li} are the total energies of Mg_mLi_n, pure HCP Mg and BCC Li, respectively. After the calculation, the derived

Table 1
Structural properties of several ordered Mg–Li phases. a is the lattice constant, ΔE is the structural energy difference and ΔH_f is the heat of formation.

Phase	Structure	a (Å)		c/a		ΔE (eV/atom)	ΔH_f (kJ/mol)	
		This work	Exp.[a]	This work	Exp.[a]		This work	Exp.[b]
Mg	BCC	3.583				0.0235		
	FCC	4.528				0.0061		
	HCP	**3.187**	**3.2095**	**1.6297**	**1.6234**	**0**		
Mg_3Li	BCC	**3.504**	**3.51**			**0**	−4.28	−2.50
	FCC	4.449				0.0192	−2.43	
	HCP	3.170	3.196[c]	1.6000	1.605[c]	0.0065	−3.36	
MgLi	BCC	**3.440**	**3.486**			0	−6.53	−3.20
	FCC	4.373				0.0217	−4.35	
	HCP	3.090		1.6220		0.0339	−3.28	
$MgLi_3$	BCC	3.439	3.5005			0.0020	−3.28	−2.00
	FCC	**4.336**	**4.37**[c]			0	−3.48	
	HCP	3.068	3.12[c]	1.6403	1.638[c]	0.0010	−3.39	
Li	BCC	3.445	3.510			0.0015		
	FCC	**4.321**	**4.379**			0		
	HCP	3.068	3.111	1.6135	1.637	0.0008		

The bold values denote the ground-state structure of various phases.
[a] Ref. [25].
[b] Ref. [28] (obtained in liquid phase).
[c] Linear extrapolation from experimental data.

values of ΔH_f for various Mg–Li phases are all listed in Table 1. It can be seen from this table that the values of ΔH_f are all negative, and the most stable structure has the lowest ΔH_f. Such negative values of ΔH_f imply that all the three common structures of Mg–Li phases would be energetically favorable from the point of view of thermodynamics, and the most stable structure with the lowest ΔH_f would be the most likely to be formed during experiments, which match well with experimental observations in the literature [25]. Due to the absence of experimental ΔH_f of solid Mg–Li phases, the experimental ΔH_f of liquid MgLi phases [29] are also included in Table 1 for the sake of comparison. It is of interest to see that the ΔH_f of the FCC Mg_3Li and HCP MgLi phases from the present study are −2.43 and −3.28 kJ/mol, respectively, which are very close to the experimental values of −2.50 and −3.20 kJ/mol of the corresponding liquid phases [29], respectively. Note that both structures are the most unstable structures with the highest energies among these three structures, such a feature of ΔH_f suggests that the FCC Mg_3Li and HCP MgLi phases should be very close to their corresponding liquid phases from the point view of the phase diagram, and that the present calculated results regarding ΔH_f would be in good agreement with experimental observations.

To find out the intrinsic mechanism of the Mg–Li interaction, the electronic structures of all Mg–Li phases are also calculated. As a typical example, Fig. 3 shows the total densities of states (DOSs) of the BCC MgLi as well as the mechanical mixture of 50 at.% Mg and 50 at.% Li bulks (without any Mg–Li interaction). Several characteristics can be seen from this figure. First, compared with the mechanical mixture, the DOSs of the BCC MgLi become more localized with a bandwidth reduction of about 2 eV, signifying that a strong chemical bonding is formed between Mg and Li atoms. Second, due to the Mg–Li interaction, two peaks of DOSs of the BCC MgLi phase appear at the points of about 1 and 3 eV below the Fermi level (E_f), and the maximum peak of DOSs above the E_f is split into several peaks. Third, there is a negligible difference between these two DOSs at the E_f.

3.2. Mechanical properties

The theoretical elastic constants of Mg–Li phases are calculated according to the method adopted by Wang and Ye [30], and the main idea is presented as follows: we apply small strains to the equilibrium lattice, determine the resulting change in total energy, and from this information, then deduce the elastic constants through quadratic polynomial fittings. Consequently, Table 2 lists the derived elastic constants of several ground-state and room-temperature structures, as well as available experimental results regarding the elastic constants of Mg–Li phases in the literature [11,12,31]. It could be seen clearly from this table that the calculated elastic constants of Mg–Li phases from the present study are in good agreement with corresponding experimental values in the literature [11,12,31]. For instance, the C_{11}, C_{12}, and C_{44} of the BCC Mg_3Li phase are calculated to be 41.7, 24.8, and 36.4 GPa, respectively, which match well with corresponding experimental values of 41, 24, and 37 GPa, respectively [12]. It should also be pointed out that FCC is the ground-state structure of $MgLi_3$ and pure Li at low temperature, while there are no any experimental results of elastic constants for these ground-state FCC structures available in the literature. Instead, the experimental elastic constants of room-temperature BCC structures of $MgLi_3$ and pure Li are therefore used for comparison in Table 2.

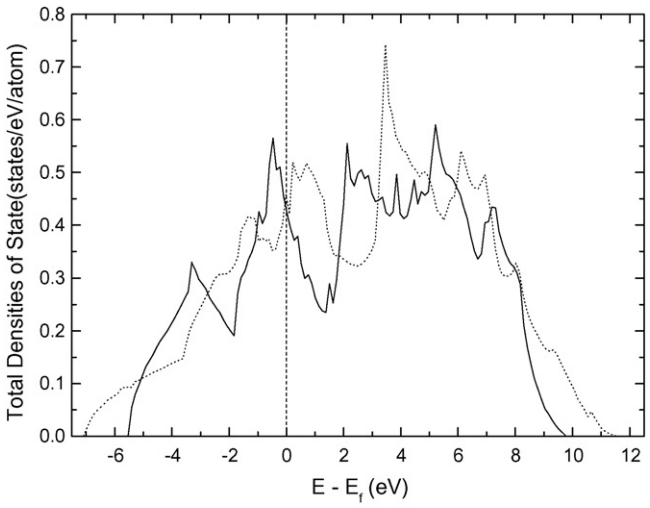

Fig. 3. Total densities of states (DOSs) of BCC MgLi (solid line) and mechanical mixture of 50 at.% Mg and 50 at.% Li pure bulks (dotted line), respectively.

Table 2
Elastic constants of single crystals and elastic moduli of polycrystalline Mg–Li phases. B is bulk modulus, G is shear modulus, E is Young's modulus, and ν is Poisson's ratio. All values, except ν, are in the unit of GPa.

Phase	Structure	Type	C_{11}	C_{12}	C_{13}	C_{33}	C_{44}	B	G	E	ν
Mg	HCP	Present	49.7	24.4	26.8	59.7	16.1	35.0	14.3	37.7	0.32
		Exp.[a]	59.50	26.12	21.80	61.55	16.35	34.3			
Mg_3Li	BCC	Present	41.7	24.8			36.4	30.5	20.4	50.1	0.23
		Exp.[b,c]	41.0	24.0			37	29.7			
	FCC	Present	29.5	28.2			27.5	28.7	9.1	24.7	0.36
MgLi	BCC	Present	34.1	20.0			26.5	24.7	15.7	38.8	0.24
		Exp.[b,c]	30.5	19.5			23.4	23.2			
	HCP	Present	9.6	48.3	12.6	44.4	11.1	23.4	18.1	43.1	0.19
$MgLi_3$	BCC	Present	22.7	16.1			13.8	18.3	7.8	20.5	0.31
		Exp.[b,c]	19.2	15.0			11.3	16.4			
	FCC	Present	22.4	16.3			17.3	18.3	8.8	22.7	0.29
Li	BCC	Present	15.1	12.7			11.4	13.5	4.9	13.1	0.34
		Exp.[d]	14.54	12.04			11.58	12.95			
	FCC	Present	15.3	12.5			8.0	13.5	4.1	11.1	0.36

[a] Ref. [11].
[b] Ref. [12].
[c] Linear extrapolation from experimental data.
[d] Ref. [30].

It is of interest to investigate the mechanical stability of various Mg–Li phases. According to the strain energy theory, for a mechanically stable phase the strain energy should be positive, and the matrix of elastic constants should be positive, definite, and symmetric [32]. This theory could be expressed for the cubic structure as: $C_{11} > 0$, $C_{11}^2 > C_{12}^2$, and $C_{44} > 0$, and for the HCP structure as: $C_{11} > 0$, $C_{11}^2 > C_{12}^2$, $C_{33}(C_{11} + C_{12}) > 2C_{13}^2$, and $C_{11}C_{33} > C_{13}^2$. Through a careful calculation, it can be deduced from Table 2 that the elastic constants of various Mg–Li phases, except HCP MgLi, all follow the above strain energy theory, suggesting that these phases should be all mechanically stable. Such a mechanically stable feature seems consistent with the thermodynamic stability of various Mg–Li phases with negative heats of formation shown in Table 1. It should be pointed out that the HCP MgLi phase listed in Table 2 possesses an anomalous mechanical instability, which will be discussed in Section 3.3. In addition, it is also of interest to find out the values of the shear coefficients $(C_{11}–C_{12})/2$ for the BCC Mg–Li phases, as proposed by Zener [33], a small value of $(C_{11}–C_{12})/2$ signifies that the BCC lattice is prone to transform to FCC or other structures through the shear of $(1\,1\,0)\,[1\,\bar{1}\,0]$. Consequently, the calculated values of $(C_{11}–C_{12})/2$ for the BCC Li, $MgLi_3$, MgLi, and Mg_3Li phases are 1.2, 3.3, 7.1, and 8.95 GPa, respectively. The small values of $(C_{11}–C_{12})/2$ for the BCC Li and $MgLi_3$ phases suggest that a phase transformation would probably happen in the BCC Li-rich region, which is in good agreement with the experimental observations of martensitic transformations in the BCC Li-rich Mg–Li phases [1–3]. It should be pointed out that the values of $(C_{11}–C_{12})/2$ for the BCC Mg–Li phases from the present study are consistent with the corresponding experimental data in the literature [12,31].

It is of engineering importance to derive the elastic moduli of polycrystalline materials, which could be approximately estimated from elastic constants of the single crystals through Voigt's and Reuss's approximations for maximum and minimum values of the moduli as well as Hill's approximation for the average value of maximum and minimum values [34], respectively.

The Voigt's (G_V), Reuss's (G_R), and Hill's (G) approximations are given as follows:

$$G_V = \frac{1}{15}(C_{11} + C_{22} + C_{33}) - \frac{1}{15}(C_{12} + C_{13} + C_{23}) + \frac{1}{5}(C_{44} + C_{55} + C_{66}) \quad (2)$$

$$G_R = \frac{15}{4}(S_{11} + S_{22} + S_{33})^{-1} - \frac{15}{4}(S_{12} + S_{13} + S_{23})^{-1} + 5(S_{44} + S_{55} + S_{66})^{-1} \quad (3)$$

$$G = \frac{1}{2}(G_V + G_R) \quad (4)$$

where S_{ij} is the compliance matrix obtained by $S_{ij} = C_{ij}^{-1}$.

The Young's modulus (E) and Poisson's ratio (ν) are expressed according to the following formulas:

$$E = \frac{9BG}{3B + G} \quad (5)$$

$$\nu = \frac{3B - E}{6B} \quad (6)$$

As a result, the calculated B, G, E, and ν of the Mg–Li phases with various polycrystalline structures are displayed in Table 2. For a detailed comparison, Fig. 4 shows various bulk moduli of polycrystalline Mg–Li phases from the present study as well as experimental

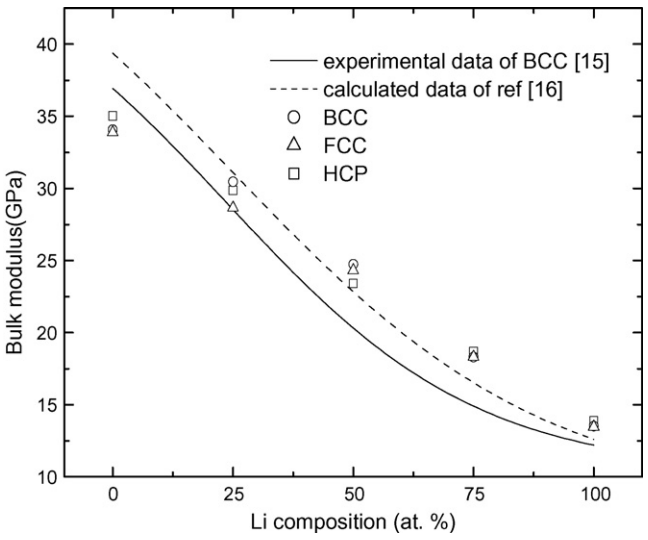

Fig. 4. Comparison of various bulk moduli of polycrystalline MgLi phases from the present study as well as experimental and theoretical data in the literature [15,16].

Table 3
Critical ratios of volume (V/V_0) and values of pressures fitted from the Vinet's EOS [41] for various phase transitions of Mg_3Li and MgLi phases, respectively.

Phase	BCC → FCC		BCC → HCP		HCP → FCC	
	V/V_0	Pressure (GPa)	V/V_0	Pressure (GPa)	V/V_0	Pressure (GPa)
Mg_3Li	0.87	3.0	~1.0	~0.0	0.69	18.3
MgLi	0.39	100.7	0.28	258.5	–	–

and theoretical data in the literature [15,16]. It can be clearly seen from this figure that the values of bulk moduli from different methods are in good agreement with each other, and that there is an almost linear relationship between bulk moduli and composition. It should be noted that for the BCC Mg–Li phases the present values of bulk moduli as well as the linear relationship also match well with the recent calculated results by Counts et al. [18]. It can be also observed that at a certain composition the bulk moduli of Mg–Li with different structures are close to each other, implying that crystal structure has only a little effect on bulk moduli of Mg–Li phases.

3.3. High-pressure phase transition

High pressure is known to influence electronic structure and crystal packing, and plays an important role in materials properties, such as phase transition, superconducting phenomenon, etc. For instance, Li, as the simplest metal, has received considerable attention in terms of high-pressure behavior [35–38]. Very recently, first principle calculation was used to study various Li–Be phases under high pressure, and the results show that the equilibrium immiscible Li–Be phases become stable or superconducting states at high pressure with interesting electronic structures [39,40]. It should be pointed out that Mg, as another alkaline-earth metal, has similar properties like Be, and it is, therefore, of importance to reveal the high-pressure phase transition of the Mg–Li system through first principles calculation.

In the present study, the Mg_3Li, MgLi, and $MgLi_3$ phases are selected to find out phase transitions under hydrostatic pressure between the common BCC, FCC, and HCP structures. The total energy is calculated as a function of the ratio of the volume (V/V_0) which ranges from 1.55 to 0.2 with an interval of 0.04. The derived total energies of the three phases with various structures are then fitted through the Vinet's equation of state (EOS) [41] to determine the pressure values corresponding to different volume changes. It should be noted that the Vinet's EOS, instead of other forms of EOS, is purposely selected for the present fitting as it has good performance for the phase under high pressure.

After the calculation, it is found that for the $MgLi_3$ phase there is no any high-pressure phase transitions between FCC (ground-state structure), BCC and HCP structures (figures no shown). For the Mg_3Li and MgLi phases, the energy differences (ΔE) of the FCC and HCP structures with respect to the BCC structure are derived and the results are shown in Fig. 5. It can be seen from this figure that the ΔE curves as well as the line of zero intersect with each other, and that these intersections could be regarded as the critical points corresponding to the phase transitions under pressure. By means of fitting, the Vinet's EOS is then used to derive the critical pressures corresponding to the above points of phase transitions, and the calculated results are all listed in Table 3. Several characteristics can be observed from Fig. 5 and Table 3. First, it can be deduced from Fig. 5(a) that Mg_3Li has a phase sequence of BCC → HCP → FCC under pressure. In other words, the BCC structure, i.e., the most stable structure of Mg_3Li under normal conditions, is first transformed to the HCP structure, and then to the FCC structure with the increase of pressure. Second, it is of interest to see that for the transition of BCC to HCP in the Mg_3Li phase, the critical volume is almost coincident with the equilibrium volume and the corresponding pressure is very close to zero. Such a feature suggests that the transition from BCC to HCP would be very easily achieved for the Mg_3Li phase, which is in excellent agreement with the coexistence of these two structures from the experimentally observed phase diagram of Mg–Li [25]. Third, it can be observed from Table 3 that the critical ratios of volume corresponding to the phase transitions of the MgLi phase are much lower, and the critical pressures are significantly higher than those of the Mg_3Li phase, implying that the high-pressure phase transitions of the MgLi phase would be much more difficult to happen than those of the Mg_3Li phase. Forth, it could be seen from Fig. 5(b) that MgLi has a phase sequence of BCC → FCC under pressure, which is quite different from that of Mg_3Li. It should be pointed out that although there is an intersection between the HCP and BCC curves in Fig. 5(b), the transition from BCC to HCP for the MgLi phase could not actually happen under pressure as the transition from BCC to FCC would happen first within the entire range of V/V_0, and there is no any intersection between the HCP and FCC curves. In other words, neither BCC

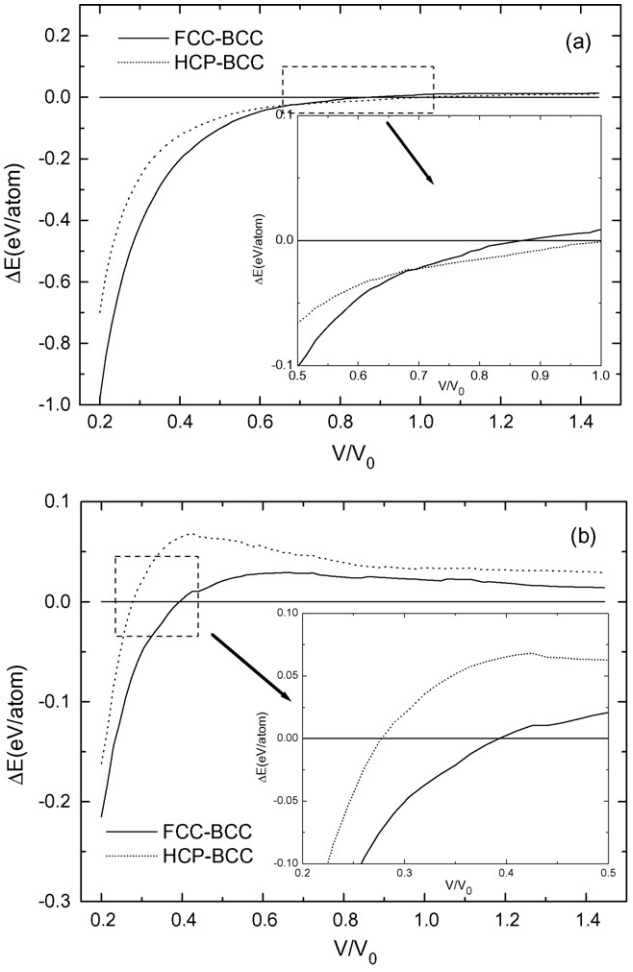

Fig. 5. Energy differences (ΔE) of FCC (solid lines) and HCP (dotted lines) structures with respect to BCC for (a) Mg_3Li and (b) MgLi phases under various volume changes, respectively.

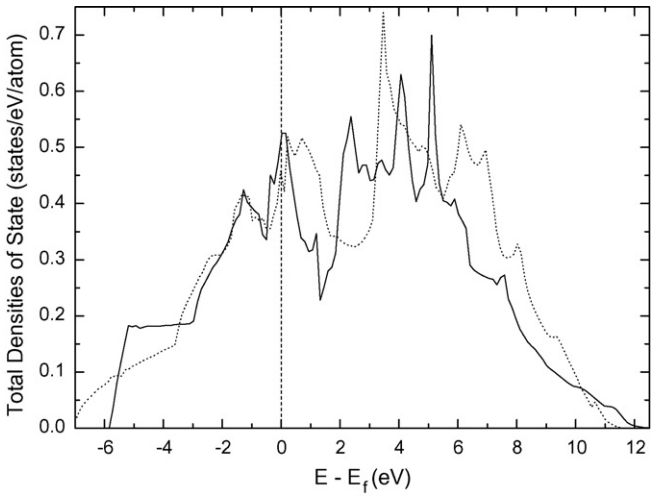

Fig. 6. Total densities of states (DOSs) of HCP MgLi (solid line) and mechanical mixture of 50 at.% Mg and 50 at.% Li pure bulks (dotted line), respectively.

nor FCC MgLi could be transformed to the HCP structure, suggesting that the HCP MgLi could not be obtained even under high pressure.

It is of interest to find out the anomaly of the HCP MgLi phase. From Table 1, it can be seen that the heat of formation of the HCP MgLi is calculated to be −3.28 kJ/mol, suggesting that the HCP MgLi phase should be thermodynamically favorable. As related in Section 3.2, however, it could be deduced from Table 2 that the HCP MgLi is mechanically unstable as it disobeys the strain energy theory of $C_{11}{}^2 > C_{12}{}^2$ [32]. Furthermore, from Fig. 5(b) as well as the above analyses of high-pressure behavior, the HCP MgLi is identified to be unstable even under high pressure. It should be noted that such an anomalous behavior regarding the stability of the HCP MgLi phase is quite different from those of other MgLi phases. To get a better understanding of the HCP MgLi phase, the electronic structure of the HCP MgLi is calculated, and Fig. 6 shows the comparison of the total densities of states (DOSs) of the HCP MgLi as well as the mechanical mixture of 50 at.% Mg and 50 at.% Li bulks (without any Mg–Li interaction). One sees from this figure that the DOSs of the HCP MgLi are similar to those of its mechanical mixture in terms of the bandwidth, shape, and the peaks of the DOSs, etc., implying that the HCP structure of MgLi should have a weak bonding. Interestingly, the DOSs of the HCP structure have a remarkable step-like feature near the bottom of the valence band and it remains almost constant within the energy range of −5.5 to −3 eV. Such an unusual electronic structure of the HCP MgLi phase would be probably due to large size differences between the ionic cores of Li and Mg, i.e., as the density increases under pressure, the Li cores start to overlap and thereby expel valence electrons into delocalized free-particle-like states in the vicinity of Mg ions [39]. It should be emphasized that the above unusual electronic structure of the HCP MgLi phase from the present study is very similar to those of the high-pressure Li–Be phases in two recent publications [39,40]. It should be also noted that the weak bonding and step-like feature of DOSs would probably give a reasonable explanation to the mechanical instability of HCP MgLi phase revealed from the present study.

4. Concluding remarks

In the present study, first principle calculation has been conducted to investigate the structural stabilities, mechanical properties, and high-pressure phase transitions of the Mg–Li system. It is demonstrated that first principle calculation is able to reveal various physical properties of MgLi phases, such as the lattice constants, heats of formation, total energy differences, elastic constants, bulk moduli, mechanical stabilities, phase transitions under high pressure, etc. It is also shown that the electronic structures of the MgLi phases from the present first principle calculation would give a deeper understanding of various properties of the MgLi phases. In addition, the calculated results are compared with experimental evidences in the literature, and the agreements between them are fairly good.

Acknowledgments

This research work is supported by National Natural Science Foundation of China (Grant No. 50871124) and Creative research group of National Natural Science Foundation of China (Grant No. 50721003).

References

[1] C.S. Barrett, Phys. Rev. 72 (1947) 245.
[2] C.S. Barrett, O.R. Trautz, Trans. Am. Inst. Mining Metall. Petrol. Eng. 175 (1948) 579.
[3] C.S. Barrett, Acta Metall. 4 (1956) 528.
[4] R.S. Crisp, J. Phys.: Condens. Matter 3 (1991) 5761.
[5] Ch. Maier, O. Blaschko, W. Pichl, Phys. Rev. B 51 (1995) 779.
[6] A.M. Russell, L.S. Chumbley, V.B. Gantovnik, K. Xu, Y. Tian, F.C. Laabs, Scr. Mater. 39 (1998) 1663;
J.F. King, Mater. Sci. Technol.-Lond. 27 (2007) 1.
[7] J.F. Mason, C.M. Warwick, P.J. Smith, J.A. Charles, T.W. Clyne, J. Mater. Sci. 24 (1989) 3934.
[8] G.J. Shen, B.J. Duggan, Metall. Trans. A 38 (2007) 2593.
[9] S.R. Agnew, M.H. Yoo, C.N. Tomé, Acta Mater. 49 (2001) 4277.
[10] M. Furui, C. Xu, T. Aida, M. Inoue, H. Anada, T.G. Langdon, Mater. Sci. Eng. A 410–411 (2005) 439.
[11] A.R. Wazzan, L.B. Robinson, Phys. Rev. 155 (1967) 586.
[12] M.E. Siedersleben, S. Naito, G. Taylor, Philos. Mag. B 67 (1993) 3.
[13] K. Liu, M. Zhang, J. Zhai, J. Wang, L. Jiang, Appl. Phys. Lett. 92 (2008) 183103.
[14] G.D. Oomi, M.A.K. Mohammed, S.B. Woods, Solid State Commun. 53 (1985) 223; G. Punz, J. Hafner, Z. Phys. B: Condens. Matter 65 (1987) 465.
[15] R.W. Lynch, L.R. Edwards, J. Appl. Phys. 41 (1970) 5135.
[16] J. Hafner, J. Phys. F: Met. Phys. 6 (1976) 1243.
[17] J. Hafner, W. Weber, Phys. Rev. B 33 (1986) 747.
[18] W.A. Counts, M. Friák, D. Raabe, J. Neugebauer, Acta Mater. 57 (2009) 69.
[19] I.A. Abrikosov, Y.H. Vekilov, P.A. Korzhavyi, A.V. Ruban, L.E. Shilkrot, Solid State Commun. 83 (1982) 867;
T. Uesugi, M. Kohyama, M. Kohzu, K. Higashi, Mater. Sci. Forum 350–351 (2000) 49.
[20] G. Kresse, J. Hafner, Phys. Rev. B 47 (1993) 558.
[21] G. Kresse, J. Joubert, Phys. Rev. B 59 (1999) 1758.
[22] J.P. Perdew, J.A. Chevary, S.H. Vosko, K.A. Jackson, M.R. Pederson, D.J. Singh, C. Fiolhais, Phys. Rev. B 46 (1992) 6671.
[23] M. Methfessel, A.T. Paxton, Phys. Rev. B 40 (1989) 3616.
[24] P.E. Blöchl, O. Jepsen, O.K. Andersen, Phys. Rev. B 49 (1994) 16223.
[25] A.A. Nayeb-Hashemi, J.B. Clark, A.D. Pelton, Bull. Alloy Phase Diagrams 5 (1984) 365.
[26] J.S. Dugdale, D. Gugan, H.H. Wills, Cryogenics 2 (1961) 103.
[27] P. Staikov, A. Kara, T.S. Rahman, J. Phys.: Condens. Matter 9 (1997) 2135.
[28] J.C. Boettger, S.B. Trickey, Phys. Rev. B 32 (1985) 3391.
[29] F. Sommer, Z. Metallkd. 70 (1979) 359.
[30] S.Q. Wang, H.Q. Ye, J. Phys.: Condens. Matter 15 (2003) 5307.
[31] R.A. Felice, J. Trivisonno, D.E. Schuele, Phys. Rev. B 16 (1977) 5173.
[32] M.H. Sadd, ELASTICITY: Theory, Applications, Numerics United States of America, Elsevier Inc., 2005, pp. 291–292.
[33] C. Zener, Phys. Rev. 71 (1947) 846.
[34] J.H. Westbrook, R.L. Fleischer (Eds.), Intermetallic Compounds: Principles Practice, vol. I: Principles London, John Wiley Sons, 1995, Ch. 1, Ch. 9.
[35] B. Olinger, W. Shaner, Science 219 (1983) 1071.
[36] M. Hanfland, K. Syassen, N.E. Christensen, D.L. Novikov, Nature (London) 408 (2000) 174.
[37] J.B. Neaton, N.W. Ashcroft, Nature (London) 400 (1999) 141.
[38] Y. Ma, A.R. Oganov, Y. Xie, Phys. Rev. B 78 (2008) 14102.
[39] J. Feng, G.H. Richard, N.W. Ashcroft, R. Hoffmann, Nature (London) 451 (2008) 445.
[40] I. Errea, M. Martinez-Canales, A. Bergara, Phys. Rev. B 78 (2008) 172501.
[41] P. Vinet, J. Ferrante, J.R. Smith, J.H. Rose, J. Phys. C 19 (1986) L467.